Research Article | Vol. 25, No. 17 | 21 Aug 2017 | OPTICS EXPRESS 20313

Optics EXPRESS

Surface plasmon resonance biosensor based on gold-coated side-polished hexagonal structure photonic crystal fiber

TIESHENG WU,[1,2] YU SHAO,[1] YING WANG,[1,3] SHAOQING CAO,[1] WEIPING CAO,[2] FENG ZHANG,[1] CHANGRUI LIAO,[1] JUN HE,[1] YIJIAN HUANG,[1] MAOXIANG HOU,[1] AND YIPING WANG[1,4]

[1]*Key Laboratory of Optoelectronic Devices and Systems of Ministry of Education and Guangdong Province, College of Optoelectronic Engineering, Shenzhen University, Shenzhen 518060, China*
[2]*Guangxi Key Laboratory of Wireless Broadband Communication and Signal Processing, Guilin University of Electronic Technology, Guilin 541004, China*
[3]*yingwang@szu.edu.cn*
[4]*ypwang@szu.edu.cn*

Abstract: The refractive index sensing characteristics of the side-polished photonic crystal fiber (PCF) surface plasmon resonance (SPR) sensor are detailed investigated in this paper. We used the finite element method (FEM) to study the influences of the side-polished depth, air hole size, lattice constant, and the refractive index (RI) of the PCF material on sensing performance. The simulation results show that the side-polished depth, air hole size, lattice pitch have significant influence on the coupling strength between core mode and surface plasmon polaritons (SPPs), but have little influence on sensitivity; the coupling strength and sensitivity will significant increase with the decrease of RI of the PCF material. The sensitivity of the D-shaped PCF sensor is obtained to be as high as 21700 nm/RIU in the refractive index environment of 1.33-1.34, when the RI of the PCF material is controlled at 1.36. It revealed a new method of making ultra-high sensitivity SPR fiber sensor. Then we experimental demonstrated a SPR refractive sensor based on the side-polished single mode PCF and investigated the sensing performance. The experimental results of the plasmon resonance wavelength sensitivity agree well with the theoretical results. The presented gold-coated D-shaped PCF SPR sensor could be used as a simple, cost-effective, high sensitivity device in bio-chemical detection.

OCIS codes: (060.2370) Fiber optics sensors; (240.6680) Surface plasmons; (060.5295) Photonic crystal fibers; (280.4788) Optical sensing and sensors.

References and links

1. A. Hassani and M. Skorobogatiy, "Design criteria for microstructured-optical-fiber-based surface plasmon resonance sensors," J. Opt. Soc. Am. B **24**(6), 1423–1429 (2007).
2. R. C. Jorgenson and S. S. Yee, "A fiber optic chemical sensor based on surface plasmon resonance," Sens. Actuators B Chem. **12**(3), 213–220 (1993).
3. R. Slavík, J. Homola, and J. Čtyroký, "Single-mode optical fiber surface plasmon resonance sensor," Sens. Actuators B Chem. **54**(1), 74–79 (1999).
4. D. F. Santos, A. Guerreiro, and J. M. Baptista, "SPR microstructured D-type optical fiber sensor configuration for refraction index measurement," IEEE Sens. J. **15**(10), 5472–5476 (2015).
5. B. Lee, S. Roh, and J. Park, "Current status of micro- and nano-structured optical fiber sensors," Opt. Fiber Technol. **15**(3), 209–221 (2009).
6. J. Kondoh, M. Sugimoto, Y. Matsui, and H. Suzuki, "Effects of gold film thickness on spectrum profile and sensitivity of a multimode-optical-fiber SPR sensor," Sens. Actuators B Chem. **132**(1), 26–33 (2008).
7. Z. H. Liu, Y. Wei, Y. Zhang, Z. D. Zhu, E. M. Zhao, Y. X. Zhang, J. Yang, C. Y. Liu, and L. B. Yuan, "Reflective-distributed SPR sensor based on twin-core fiber," Opt. Commun. **366**, 107–111 (2016).
8. Z. Liu, Y. Wei, Y. Zhang, Y. Zhang, E. Zhao, J. Yang, and L. Yuan, "Twin-core fiber SPR sensor," Opt. Lett. **40**(12), 2826–2829 (2015).
9. D. Monzón-Hernández and J. Villatoro, "High-resolution refraction index sensing by means of a multiple-peak surface plasmon resonance optical fiber sensor," Sens. Actuators B Chem. **115**(1), 227–231 (2006).

#300781 https://doi.org/10.1364/OE.25.020313
Journal © 2017 Received 22 Jun 2017; revised 1 Aug 2017; accepted 2 Aug 2017; published 11 Aug 2017

Optics EXPRESS

10. M. Tian, P. Lu, L. Chen, C. Lv, and D. Liu, "All-solid D-shaped photonic fibber sensor based on surface plasmon resonance," Opt. Commun. **285**(6), 1550–1554 (2012).
11. N. Luan, R. Wang, W. Lv, and J. Yao, "Surface plasmon resonance sensor based on D-shaped microstructured optical fiber with hollow core," Opt. Express **23**(7), 8576–8582 (2015).
12. H. L. Chen, S. Q. Li, G. W. An, J. S. Li, Z. K. Fan, and Y. Han, "Polarization splitter based on d-shaped dual-core photonic crystal fibers with gold film," Plasmonics **10**(1), 57–61 (2015).
13. M. H. Chiu, S. F. Wang, and R. S. Chang, "D-type fiber biosensor based on surface-plasmon resonance technology and heterodyne interferometry," Opt. Lett. **30**(3), 233–235 (2005).
14. Z. Tan, X. Hao, Y. Shao, Y. Chen, X. Li, and P. Fan, "Phase modulation and structural effects in a D-shaped all-solid photonic crystal fiber surface plasmon resonance sensor," Opt. Express **22**(12), 15049–15063 (2014).
15. A. Patnaik, K. Senthilnathan, and R. Jha, "Graphene-based conducting metal oxide coated D-shaped optical fiber SPR sensor," IEEE Photonics Technol. Lett. **27**(23), 2437–2440 (2015).
16. Y. J. He, "Novel D-shape LSPR fiber sensor based on nano-metal strips," Opt. Express **21**(20), 23498–23510 (2013).
17. B. Spacková and J. Homola, "Theoretical analysis of a fiber optic surface plasmon resonance sensor utilizing a Bragg grating," Opt. Express **17**(25), 23254–23264 (2009).
18. Y. Zhao, Z. Q. Deng, and J. Li, "Photonic crystal fiber based surface plasmon resonance chemical sensors," Sens. Actuators B Chem. **202**, 557–567 (2014).
19. Q. L. Xie, Y. Z. Chen, X. J. Li, Z. Yin, L. L. Wang, Y. F. Geng, and X. M. Hong, "Characteristics of D-shaped photonic crystal fiber surface plasmon resonance sensors with different side-polished lengths," Appl. Opt. **56**(5), 1550–1554 (2017).
20. Y. Z. Chen, Q. L. Xie, X. J. Li, H. S. Zhou, X. M. Hong, and Y. F. Geng, "Experimental realization of D-shaped photonic crystal fiber SPR sensor," J. Phys. D Appl. Phys. **50**(2), 025101 (2017).
21. L. Peng, F. K. Shi, G. Y. Zhou, S. Ge, Z. Y. Hou, and C. M. Xia, "A surface plasmon biosensor based on a D-shaped microstructured optical fiber with rectangular lattice," IEEE Photonics J. **7**(5), 1–9 (2015).
22. C. Z. Tan, "Determination of refractive index of silica glass for infrared wavelengths by IR spectroscopy," J. Non-Cryst. Solids **223**(1-2), 158–163 (1998).
23. P. B. Johnson and R. W. Christy, "Optical Constants of the Noble Metals," Phys. Rev. B **6**(12), 4370–4379 (1972).
24. T. Wu, Y. Liu, Z. Yu, Y. Peng, C. Shu, and H. Ye, "The sensing characteristics of plasmonic waveguide with a ring resonator," Opt. Express **22**(7), 7669–7677 (2014).
25. H. L. Chen, S. G. Li, M. J. Ma, Z. K. Fan, and Y. D. Wu, "Ultrabroad bandwidth polarization filter based on D-shaped photonic crystal fiber with gold film," Plasmonics **10**(5), 1239–1242 (2015).
26. R. Otupiri, E. K. Akowuah, S. Haxha, H. Ademgil, and A. Aggoun, "A novel birefrigent photonic crystal fiber surface plasmon resonance biosensor," IEEE Photonics J. **6**(4), 6801711 (2014).
27. R. Otupiri, E. K. Akowuah, and S. Haxha, "Multi-channel SPR biosensor based on PCF for multi-analyte sensing applications," Opt. Express **23**(12), 15716–15727 (2015).
28. J. Zhao, S. Q. Cao, C. R. Liao, Y. Wang, G. J. Wang, X. Z. Xu, C. L. Fu, G. W. Xu, J. R. Lian, and Y. P. Wang, "Surface plasmon resonance refractive sensor based on silver-coated side-polished fiber," Sens. Actuators B Chem. **230**, 206–211 (2016).
29. X. J. Feng, M. Yang, Y. H. Luo, J. Y. Tang, H. Y. Guan, J. B. Fang, H. H. Lu, J. H. Yu, J. Zhang, and Z. Chen, "Long range surface plasmon resonance sensor based on side polished fiber with the buffer layer of magnesium fluoride," Opt. Quantum Electron. **49**(4), 147 (2017).

1. Introduction

Surface plasmon resonance technology can serve as a basis of many standard tools used to measure the extent that electromagnetic wave can be absorbed into the metal-dielectric structure (typically gold or silver with dielectric). It is extremely sensitive to changes in permittivity of the metal and dielectric, and the structural shape. This feature constitutes the core of designing high sensitivity SPR sensors [1]. During the past decade, a great effort has been devoted to adapt and optimize SPR sensing configurations based on optical fibers. Doctor Jorgenson firstly proposed the SPR fiber sensor in 1993 [2]. In order to enhance sensitivity and narrow full width at half maximum (FWHM) of resonance peak, the multimode fibers (MMF) were instead by single mode fibers (SMF) as the sensing element [3]. In many of these later fiber SPR sensing configurations, the cladding of the fiber is removed (sensing area) to allow for the deposition of a thin metallic (mostly Au or Ag) layer that supports the excitation of SPR and their interaction with optical waveguide modes of the fiber [4,5]. These configurations include the modified fiber end [6–8], tapered fiber [9], D-shaped fiber [4,10–16], fiber grating [17], and photonic crystal fiber [18]. According to the control ability of coupling between optical fiber core modes and surface plasmon waves,

Optics EXPRESS

more and more attention is being paid to the surface plasmon resonance sensor based on D-shaped photonic crystal fiber recent years.

Nowadays, the surface plasmon resonance (SPR) sensor based on microstructured optical fiber (MOF) is becoming more and more popular for having extensive application prospects in biochemical sensing field. There is, however, one downside that many researchers encounter is the difficulty in phase matching and analyte filing when dealing with MOF based SPR sensors. As an innovative solution, Luan et al. [11] proposed a MOF-based SPR sensor characterized by two special designs. One is a D-shaped hollow core that can lower the refractive index of a Gaussian-like core mode so as to match with that of a Plasmon mode. The other novelty lies with the method of depositing analyte, that is, the analyte is deposited directly onto the D-shaped flat surface rather than filling the fiber core. With this new method, they have obtained a satisfactory spectral sensitivity of 2900 nm/RIU. Later, On the basis of D-shape gold film photonic crystal fibers, Chen et al. [12] have designed an ultrabroad bandwidth polarization filter. One benefit of the structure is that it helps with generating multiple resonances between fiber waveguide modes and surface plasmon polaritons (SPPs) modes. Similar work has been conducted by others, like Tan et al. [14], who have carried out a numerical investigation on a deep-polished fiber SPR sensor, which was designed with all-solid photonic crystal fiber and found to have exhibited major phase modulation. By utilizing the phase modulation and adopting phase interrogation method, the sensitivity has been determined to be 9.09×10^4 Deg/RIU, the theoretical value is higher than those of the conventional wavelength sensitivity. It is noteworthy that Xie et al. [19,20] experimental researched the influences of side-polished depths and sensing layer thicknesses on D-shaped photonic crystal fiber surface plasmon resonance sensors, and concluded that the sensitivity increases as the sensing layer thickness increases. But it decreases slightly when the side-polished depth is going up with a certain range. Then they determined the highest sensitivity to be 7381.0nm/RIU in the refractive index environment of 1.40-1.42. Last but not least, Peng et al. [21] proposed a D-shaped MOF SPR senor, which consists of a rectangular lattice with two special large air holes. Based on the analysis of the mode coupling characteristics, the sensing performance dependence of fiber birefringence and the two large leaky channels is revealed. Theoretically, the proposed sensor improves the wavelength sensitivity with a value of 7481 nm/RIU.

In this paper, we present a SPR fiber sensor based on D-shaped photonic crystal fiber. Through numerically investigating the transmission loss for different side-polished depths, hole sizes, lattice pitches and refractive index coefficients of the material making PCF, we found that all of these parameters have significant influence on the coupling strength between y-polarized core mode and surface plasmon polaritons (SPPs), but only the RI of the PCF material has a much more significant influence on sensitivity. Simulated results indicated that high sensitivity 21700 nm/RIU is acquired in our proposed sensor model, which is higher than the theoretical values of previous reports [1–21]. Furthermore, we experimentally realize a SPR fiber sensor based on side-polished PCF. Compared to reports in [19,20], our experimental results are closer to theoretical values with improved sensing performance.

2. Theoretical analysis

The schematic diagram of the fiber SPR sensor based on D-shaped PCF in 3D view is shown in Fig. 1. All the six layers air holes are arranged in a hexagon arrangement with a lattice pitch Λ, and the diameter of the air holes is d. The upper side of the PCF is polished with a polishing depth h, which is the height of the fiber center to the polished surface, the gold film has a fixed thickness t with a value of 45 nm, and where it touches the analyte. The RI of the background material of the PCF and the gold layer are given by experimental values with linear interpolation [22,23]. To simulate the waveguide mode of the side-polished PCF SPR sensor, we use the finite element method with perfect match layers (PMLs) boundaries [24]. In this method, the Fourier components electric field of electromagnetic wave is discretized in

Optics EXPRESS

algebraic system, and then the eigenmodes are calculated. The simulation is completed by commercial software COMSOL Multiphysics [10–14]. In addition, we assume that the refractive index of the analyte changes from 1.33 to 1.34. According to definition, the wavelength sensitivity is given by [11,12]:

$$S_\lambda = \Delta\lambda_{res} / \Delta n_\alpha , \tag{1}$$

where λ_{res} is the plasmon resonance wavelength of the D-shaped PCF sensor, and n_α is the refractive index of the analyte. In the field of waveguide optics, the confinement loss is calculated according to the following equation [25]:

$$\alpha = 8.686 \cdot k_0 \, \mathrm{Im}[n_{eff}](dB/m), \tag{2}$$

where $k_0 = 2\pi/\lambda$ is the wavenumber in meter scale.

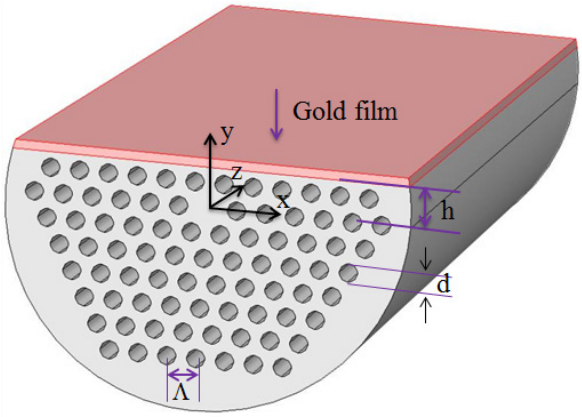

Fig. 1. Schematic diagram of the SPR sensor based on D-shaped photonic crystal fiber in 3D model. The PCF polished surface is perpendicular to the y axis.

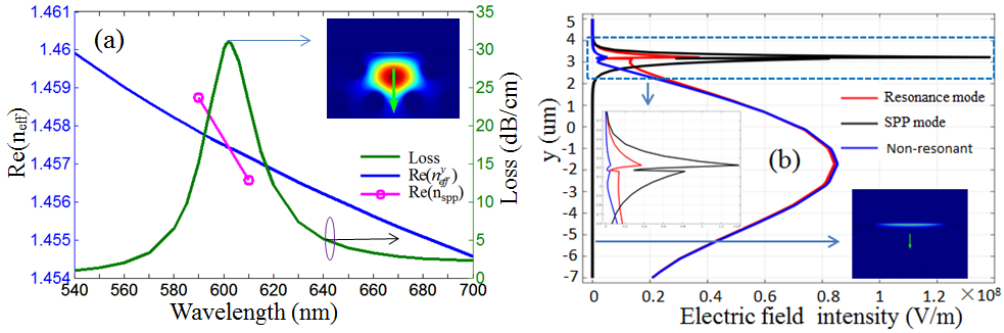

Fig. 2. (a). Real part of effective refractive index of the y-polarized fiber core mode and SPP mode, and the loss spectra of the D-shaped PCF SPR sensor with Λ = 7.8 um, d = 3.6 um, h = 0.4Λ, and n_a = 1.33. (b) Electric field distributions of the y-polarized care modes at λ = 520 nm, λ = 602 nm (phase matching point), and the SPP mode at λ = 540 nm along the y axis.

Figure 2(a) plots the real parts of the y-polarized fiber core mode, the first-order surface plasmon polaritons (SPP), and the confinement loss of the y-polarized fundamental core mode with different wavelength when n_a = 1.33, Λ = 7.8 um, d = 3.6 um, and h = 0.4Λ. As show in Fig. 2(a), with the wavelength increasing, the loss of the y-polarized fundamental core mode first increases and then decreases. When the refractive index real part of the y-polarized core mode is equal to the real value of the refractive index of the SPP mode, that is to say, it is to meet the phase matching conditions, the loss of the y-polarized core mode

Optics EXPRESS

reaches the maximum value at λ = 602 nm. To further illustrate the physical phenomenon, the electric field intensity of the y-polarized core modes at resonance wavelength λ = 602 nm [insert Fig. 2(a)], non-resonance wavelength λ = 540 nm, and the SPP mode [insert Fig. 2(b)] at λ = 540 nm are compared in the form of electric field distributions along the *y*-axis. From the Fig. 2(b), we can see that there are clear essential difference between the y-polarized core mode and the SPP mode. At different values of light wavelength, the electric field strength of the y-polarized core mode appears in near the metal film with different strength. The electric field distributions of y-polarized core mode mainly appear in the core area of the PCF. However, the electric field distributions of the SPP mode mainly appear in the interface of gold film and dielectric [insert Fig. 2(b), amplifying section]. It is clear that the y-polarized fundamental core mode and the SPP mode occurs high coupling at the wavelength of 602 nm. Since some energy of the fiber waveguide mode is transfer into the energy of the SPR mode, making the loss spectra of the fiber core mod appears a loss peak at the resonance wavelength [26,27]. The RI of the analyte has a significant influence on coupling between the y-polarized core mode and the SPP mode. With the change of the RI of the analyte, the coupling wavelength (resonance wavelength) would be to shift from one position to another. Therefore, the loss peak of the loss spectra will vary with the change of the RI of the analyte.

Next, we will discuss the sensing characteristics and the coupling characteristics of the D-shaped PCF SPR sensor. In the wavelength interrogation method, according to the relationship between the peak wavelength of the loss spectra and the RI of the analyte, the RI of the analyte under sensing can be obtained by being measured the peak wavelength of the loss spectra. This is the sensing principle of the D-shaped PCF SPR sensor.

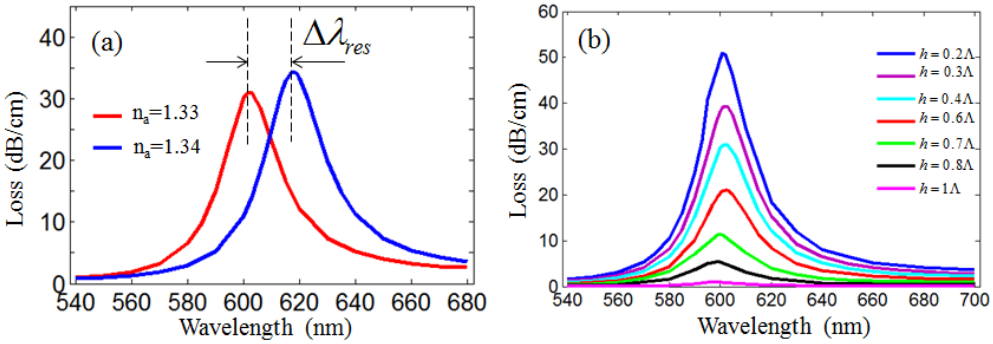

Fig. 3. (a) Loss spectra of the y-polarized core mode with analyte n_a at 1.33 and 1.34 when Λ = 7.9 um, d = 3.6 um, and h = 0.4Λ. (b) Loss spectra of the y-polarized core mode for different values of the *h* with n_a = 1.33.

Figure 3(a) presents loss spectra of the y-polarized core mode for two different RI of the sensing analyte with Λ = 7.9 um, *d* = 3.6 um, and *h* = 0.4Λ. The simulation results are shown in Fig. 3(a), with the refractive index of the sensing analyte increasing, the peak wavelength of the loss spectra exhibits a red shift and the coupling strength increases accordingly. When the RI of the sensing analyte changing from 1.33 to 1.34, the shift of the peak wavelength $\Delta\lambda_{res}$ is 16 nm, and the corresponding theoretical wavelength sensitivity of the SPR sensor is about 1600 nm/RIU. Here, we want to determine the impact of the polishing depth of D-shaped PCF on the sensing performance. Figure 3(b) illustrates loss spectra of the y-polarized core mode for different polishing depths with Λ = 7.9 um, d = 3.6 um, and n_a = 1.33. As shown in Fig. 3(b), with the polishing depth *h* decreasing, that is to say, the polishing surface is more and more closer to the fiber core, the coupling strength between y-polarized fundamental core mode and SPP mode will increase, resulting in the loss of the y-polarized fundamental core mode at resonant wavelength both increases. But the position of the resonant wavelength is almost unaffected by the polishing depth. The effect of polished depth

Optics EXPRESS

on wavelength sensitivity is described in Table 1. The results show that the wavelength sensitivity is almost unchanged when varying the polishing depth h. So we cannot improve the wavelength sensitivity by optimizing the polishing depth.

Table 1. Wavelength sensitivities (S_λ) of the D-shaped PCF SPR sensor with different h.

h	1Λ	0.8Λ	0.6Λ	0.4Λ	0.2Λ
S_λ (nm/RIU)	1500	1500	1600	1600	1700

When the duty ratio Λ of the PCF is set to be 7.9 um, the polishing depth h is set to be 0.4Λ, the RI of the sensing analyte is set to be 1.33 or 1.34, respectively, the real part of the effective refractive index (Re(n_{eff})) and the peak loss of the loss spectra of the y-polarized fundamental core mode at the resonant wavelength for different duty ratios are shown in Fig. 4(a). With the duty ratio increases, the Re(n_{eff}) of the y-polarized core mode decreases, and simultaneously the peak loss of the loss spectra increases correspondingly. But the change of Re(n_{eff}) of the y-polarized core mode at the phase matching point is so small and we cannot tune the resonance wavelength by changing the duty ratio of PCF. Table 2 describes the wavelength sensitivity for different duty ratios of PCF. As duty ratio of PCF increases, but the wavelength sensitivity of the D-shaped PCF SPR sensor does not change. Therefore the wavelength sensitivity is independent of the duty ratio of PCF.

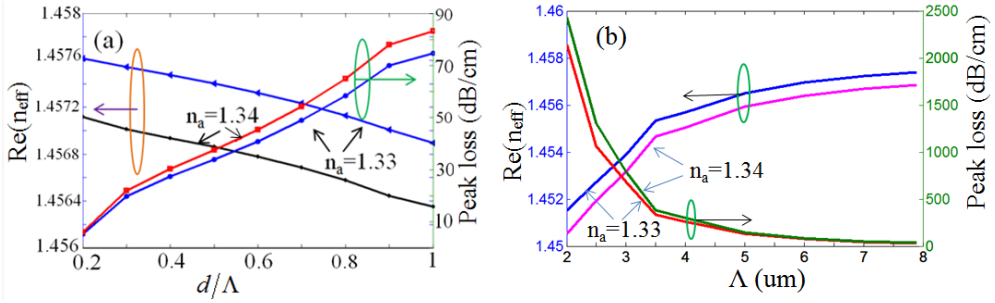

Fig. 4. The Re(n_{eff}) of the y-polarized core mode at the phase matching point and the peak loss of the y-polarized core mode for various values of (a) duty ratio with Λ = 7.9 um, and h = 0.4Λ, (b) lattice pitch with d = h = 0.5Λ.

Table 2. Wavelength sensitivities (S_λ) of the D-shaped PCF SPR sensor with different duty ratios.

d/Λ	0.2	0.3	0.4	0.5	0.6	0.7	0.8	0.9	1
S_λ (nm/RIU)	1600	1600	1600	1600	1600	1600	1600	1600	1500

Table 3. Wavelength sensitivities (S_λ) of the sensor with different lattice pitches of PCF

Λ(um)	2	3	4	5	6	7	7.9
S_λ (nm/RIU)	1800	1700	1700	1500	1600	1600	1600

Figure 4(b) illustrates the Re(n_{eff}) and the peak loss of the y-polarized fundamental core mode at the resonant wavelength for different lattice pitches. Where both of the diameter of air hole and the polishing depth are set to be 0.5Λ. When the lattice pitch of PCF Λ changes from 2 um to 7.9 um, as shown in Fig. 4(b), the Re(n_{eff}) of the y-polarized fundamental core mode at the resonant wavelength increases, but the peak loss decreases correspondingly. The results indicated that the coupling strength between the core mode and the SPP mode reduces gradually with increase of the size of lattice pitch Λ. It leads to a reduction in peak loss of the loss spectra at resonant wavelength. Table 3 shows the wavelength sensitivity of the D-shaped PCF SPR senor for different lattice pitches. With the lattice pitch of PCF increasing, the

Optics EXPRESS

sensitivity increases at first and then reduces. But the sensitivity changes little so that it is impossible to improve sensitivity by varying the lattice pitch.

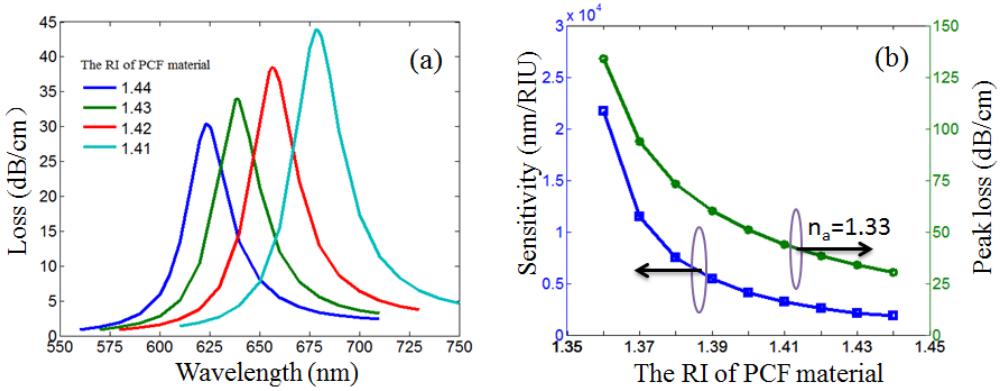

Fig. 5. (a) Loss spectra of the y-polarized core mode with the RI of PCF material at 1.44, 1.43, 1.42, and 1.41 when Λ = 7.9 um, d = 3.6 um, h = 0.5Λ, and analyte n_a = 1.33. (b) Wavelength sensitivity and peak loss of the y-polarized core mode for various values of the RI of PCF material.

As mentioned above, the wavelength sensitivity cannot be improved by varying air hole size, lattice constant of PCF, and polishing depth. Thus we would like to study the influence of the RI of PCF material on the wavelength sensitivity. Figure 5(a) depicts the loss spectra of the y-polarized fundamental core mode for different values of the RI of PCF material n = 1.44, 1.43, 1.42, and 1.41 with Λ = 7.9 um, d = 3.6 um, h = 0.5Λ, and analyte n_a = 1.33. The FEM simulation results reveal that the loss spectra of the y-polarized core mode exhibits red-shift and peak loss increases with the decreasing of the RI of PCF material. Other conditions remain unchanged, the resonant wavelength increase means that the sensitivity of the D-shaped PCF SPR sensor increases. Figure 5(b) depicts the sensitivity and peak loss of the y-polarized core mode as a function of the RI of PCF material. The RI of PCF material is varied from 1.44 to 1.36, the sensor sensitivity is extraordinary non-linear increased from 1900 nm/RIU to 21700 nm/RIU, and simultaneously the coupling strength between the y-polarized core mode and the SPP mode is increased, the latter leads to the peak loss increasing. To our best knowledge, the theoretical value of the wavelength sensitivity (21700 nm/RIU) is highest sensitivity reported in D-shaped fiber SPR senor [1–21,25,26]. Compared to these design strategies of by the introduction of a small hollow core into MOF [1,11], optimizing air holes arrayed in MOF cladding [4–10], and sensitization processing at the polished surface [27], making PCF with lower RI material is a more effective method for improving sensitivity in D-shaped fiber SPR sensor.

3. Experiment and discussion

There, we experimental demonstrate a gold-coated side-polished hexagonal structure PCF SPR sensor. ESM-12 PCF (NKT Inc.) is chosen in our experiment because it is strong enough without the tensile failure problem during the polishing process. ESM-12 PCF is an all-glass endless single-mode fiber with a standard 125 um cladding diameter. The cross section of ESM-12 PCF is shown in Fig. 6(b), the lattice constant and air hole diameter of the PCF are 7.9 um and 3.6 um, respectively. Figure 6(a) illustrates the schematic of the wheel polishing setup (Wanrun Ltd., Wuxi, China) to realize the side-polishing PCF. A 10 mm long PCF is spliced between two single-mode fibers at first and then the spliced fiber is fixed by a pair of fiber holders. In our fiber polishing system, the grinding wheel is fastened on a 3D mechanical platform that can move along the X, Y, and Z directions [28]. The polishing length and polishing depth are easy to set up and operate accurately via computer program.

Optics EXPRESS

To speed up the polishing speed, a small weight is used to straighten the fused PCF and provide suitable polishing force. Abrasive paper fastened around the mechanical wheel for polishing fiber. A broadband light source (BBS) with a range from 1250 nm to 1650 nm and an optical spectrum analyzer (OSA, Yokogawa AQ6370C) are employed to online monitoring the transmission spectrum during the polishing process [28]. The PCF polished surface is gently cleaned using an air-laid paper with water to remove residual silica dust. The polishing process is stopped at the stage when the polishing surface appears near the PCF core region and with a power loss of approximately 3 dB in air.

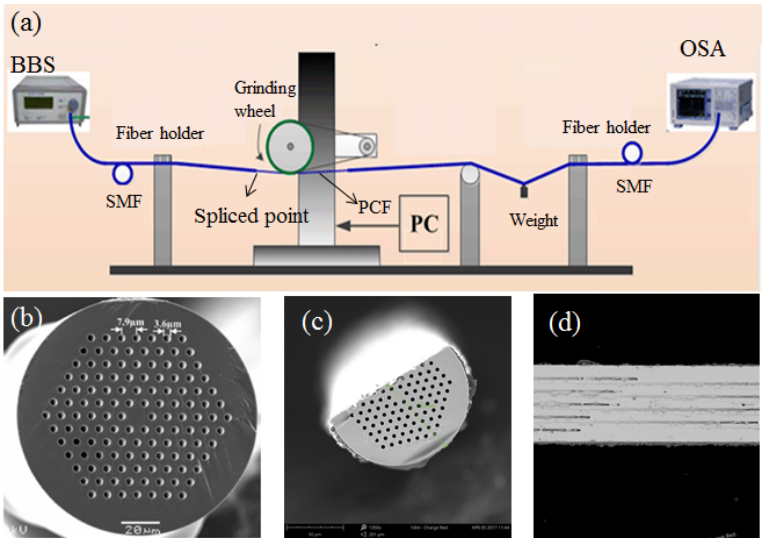

Fig. 6. (a) Optical fiber side-polised system. (b) SEM image of the PDF before polishing. (C) The cross section of the D-shaped PCF with gold-coated. (d) The side-polished surface of the D-shaped PCF with gold-coated.

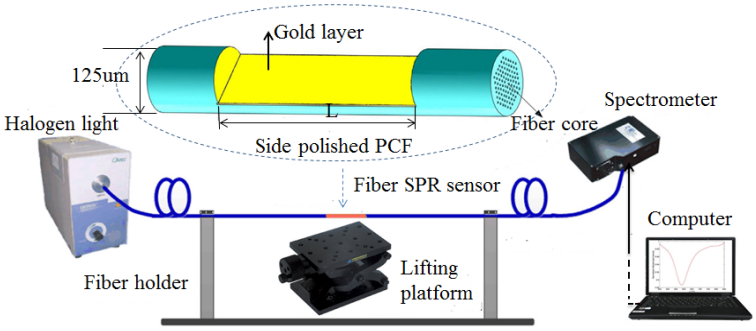

Fig. 7. Schematic diagram of the real-time online measurement system, insertion is the structure diagram of the D-shaped PCF sensor.

After completed the polishing process, Gold thin films with a thickness of 45 nm is deposited on the flat surface of the D-shaped PCF by fiber magnetron sputtering Coating machine system (LN-JS2, Shenyang Vacuum Technology Institute). Then, the work of fabricating D-shaped PCF SPR sensor is accomplished. The cross section and side-polished plane of the D-shaped PCF are observed by a microscope as shown in Figs. 6(c) and 6(d), respectively. The values of the polishing length and the polishing depth are 7mm and 13um, respectively.

In order to verify our simulation results, an experimental setup [28] for the proposed SPR sensor is presented in Fig. 7. In this sensing system, the light source is a tungsten halogen

Optics EXPRESS

with a broadband Spectrum from 450 nm to 1100 nm (LS-300, Ocean Optics Inc.), and the spectrometer is a miniature spectrometer with a measuring range from 200nm to1100nm (USB65000, Ocean Optics Inc.). The white light transmits into the SPR sensor through single mode fiber and is modulated by the refractive index matching liquids on the flat surface. Finally, the modulated optical signal is recorded at room temperature by the spectrometer. The modulated optical signal is processed by a laptop through a USB port. We need to rinse the sensor with alcohol repeatedly between each subsequent measurement to ensure that the sensing sensitive region is clean.

The experimental performance of the D-shaped PCF SPR sensor is shown in Fig. 7(a). The normalized transmission spectrum is calculated according to the ratio of the transmittance when the sensor is immersed in liquid compared to the transmittance of the sensor exposed in the air. As a result of the electromagnetic field coupling from the y-polarized fundamental core mode to SPP mode in proximity to gold film at the resonant wavelength, an obvious dip (absorption peak) appears in the transmission spectra when the sensor is immersed in each refractive index matching liquid. With the increase of the RI of the refractive index matching liquid, the dip of the transmission spectrum appears red-shift and becomes deeper. Figure 8(b) illustrates the non-liner relation between the resonance wavelength shifts versus the RI variation, where the RI of refractive index matching liquid varies of 1.30 to 1.41 with a step of 0.01. As the RI of the refractive index matching liquid increases, the wavelength sensitivity of the D-shaped PCF SPR senor non-liner increases. The results show that experimental values have a good agreement with theoretical values at lower RI of the refractive index matching liquid. In spite of rinsing the sensor with alcohol repeatedly between each subsequent measurement, it is difficult for refractive index matching liquid to be completely cleared in the air holes of PCF. This is the main source of errors between calculated results and experimental values at higher RI of refractive index matching liquid.

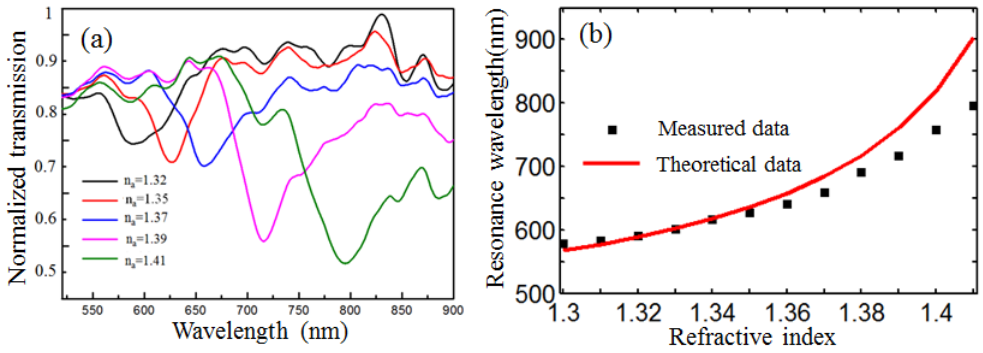

Fig. 8. (a) Experimental normalized transmission spectra of the D-shaped PCF-SPR sensor testing in different RI. (b) Experimental and theoretical values for the wavelength sensitivity.

4. Conclusion

In conclusions, we numerical and experimental investigated a D-shaped PCF-SPR sensor. The gold film and the analyte are both deposited onto the PCF polished surface. The sensing characteristics of the fiber SPR sensor and the modes coupling characteristics are analyzed by finite element method. Simulation results show that it is impossible to improve the wavelength sensitivity by changing the duty ratio, the lattice pitch of PCF, and the polishing depth. Compared to these design strategies of by the introduction of a small hollow core into MOF [1,11], optimizing air holes arrayed in MOF cladding [4–10], and sensitization processing at the polished surface [28,29], most noticeably, we proposed a more effective method for improving sensitivity in D-shaped fiber SPR sensor by making PCF or ordinary fiber with lower RI material. When the RI of PCF material is 1.36, the sensor has an extremely high sensitivity with a value of 21700 nm/RIU. In order to verify our simulation

Optics EXPRESS

results, a set of D-shaped PCF SPR sensing system is developed. The result shows that there is a good agreement between prediction of model and experiment. Considering the potential for fast-response, real-time, distributed sensing of the D-shaped fiber and these demonstrated SPR sensing characteristics. The D-shaped fiber SPR sensor based on lower RI of CPF material will be more competitive in the chemical, biological and industrial applications.

Funding

National Natural Science Foundation of China (NSFC) (No. 61675137, 61425007, and 61635007); Guangdong Natural Science Foundation (No. 2014B050504010); Science and Technology Innovation Commission of Shenzhen (No. JCYJ20160307143501276, JCYJ20150324141711611, JCYJ20150324141711614, and JCYJ20150324141711576); Education Department of Guangdong Province (No. 2015KTSCX119); Pearl River Scholar Fellowships, and the Opening Project of Guangxi Wireless Broadband Communication and Signal Processing Key Laboratory.